Journal of Superconductivity and Novel Magnetism (2022) 35:539–546
https://doi.org/10.1007/s10948-021-06102-7

ORIGINAL PAPER

Improvement of Microstructure and Magnetic Properties of Hot-Deformed Nd-Fe-B Magnets by Doping Dy-Fe Powder

Feifei Li[1] · Sajjad Ur Rehman[1] · Yikuan Hu[1] · Pengpeng Qu[1] · Shuwei Zhong[1] · Munan Yang[1,2] · Xiaoqiang Yu[1,2] · Jiajie Li[1,2]

Received: 15 October 2021 / Accepted: 7 November 2021 / Published online: 25 November 2021

Abstract
The effects of $Dy_{80}Fe_{20}$ (wt%) powder doping on the magnetic properties and thermal stability of the hot-deformed (HD) Nd-Fe-B magnets are studied. The coercivity (H_{cj}) greatly increases from 12.55 kOe for the original magnet to 18.23 kOe by doping 2 wt% $Dy_{80}Fe_{20}$ powder, which shows an increase of 45.3%. Interdiffusion occurs between the $Dy_{80}Fe_{20}$ additive and matrix phase. Dy diffuses from the $Dy_{80}Fe_{20}$ additive to the matrix phase and replaces Nd around the $Nd_2Fe_{14}B$ grains. Nd migrates into the grain boundary (GB) phase. The formation of (Nd, Dy)$_2$Fe$_{14}$B regions improves the magnetic anisotropy field (H_A) and effectively suppresses the nucleation of reverse magnetic domains. The magnetic isolation is strengthened by the improved GB phase. This explains the H_{cj} enhancement of the $Dy_{80}Fe_{20}$ doped magnet. The thermal stability of the $Dy_{80}Fe_{20}$ doped magnet is improved due to the high Curie temperature (T_C) of (Nd, Dy)$_2$Fe$_{14}$B hard magnetic phase. The relationship between recoil loops and demagnetization of the HD magnets is also discussed.

Keywords Hot-deformed magnet · Intergranular addition · Thermal stability · Microstructure · Coercivity

1 Introduction

Electric vehicles with energy-saving and emission reduction are developing rapidly due to the severe challenges posed by oil shortages in many countries. Permanent magnet motor with the characteristics of high-energy conversion efficiency and energy-saving is used as the motor for new energy vehicles [1]. Nd-Fe-B magnets are required to possess high H_{cj} at extreme working temperature (above 100 °C) [2, 3]. An effective way to improve the H_{cj} at high temperature of the magnet is to increase the H_A of $Nd_2Fe_{14}B$ phase by partially substituting Nd by heavy rare earth (HRE) Dy/Tb [4]. However, excessive HRE elements infiltrating into the interior of main phase grains dilute J_r due to the antiparallel coupling of magnetic moments between HRE and Fe [5]. Grain boundary diffusion (GBD) and intergranular addition have been proposed to improve the H_{cj} of the Nd-Fe-B magnet. For the GBD process, the HRE diffuses from the surface to the inner of the magnet after heat treatment. According to the previous reports [6–8], the formation of (Nd, HRE)$_2$Fe$_{14}$B shells after GBD increases the H_A of the magnet and suppresses the nucleation of reverse magnetic domains. The HD magnet, first reported by Lee [9], composed of hot-pressing and hot-deformation process, which is expected to obtain high-coercivity Nd-Fe-B magnets. The GBD process has been applied in HD magnets by coating low-melting-point alloy to improve the H_{cj} in recent years [10, 11]. However, a high treatment temperature (about 900 ℃) in sintered magnet is required for GBD. The grains of the HD magnet grow drastically at a high temperature. Furthermore, diffusion depth is limited and only thin magnets can be developed by applying GBD process [12].

A reliable and promising way to break the limitation of temperature and diffusion depth, intergranular addition, was proposed. Anisotropy HD magnet is prepared by mixing Nd-Fe-B magnetic powder and RE-M (M = Ga, Fe, and Cu) additive [13–15]. During the deformation process, interdiffusion occurs between powder flakes and additives. The HRE atoms diffuse from the additives to powder flakes forming (Nd, HRE)$_2$Fe$_{14}$B shells, which increases the H_A of the HD magnet. Furthermore, the magnetic isolation is

✉ Jiajie Li
lijiajie@jxust.edu.cn

[1] College of Rare Earths, Jiangxi University of Science and Technology, Ganzhou 341000, China

[2] National Rare Earth Functional Materials Innovation Center, Ganzhou 341000, China

strengthened by the formation of continuous GB phases. Tang et al. reported that the H_{cj} of HD magnet increases from the original 2.07 to 13.99 kOe by mixing MQP magnetic powder with Nd-Cu powder [16]. Sawatzki et al. found that the H_{cj} increases to 22.4 kOe with an increase of 1.7 kOe by doping DyF_3 powder [17]. It has been proved that Fe with high intrinsic saturation magnetization has positive effects on J_r [13, 18]. Therefore, in this work, we prepare anisotropic Nd-Fe-B magnet by mixing MQU-M magnetic powder with $Dy_{80}Fe_{20}$ powder. It is desired to obtain higher H_{cj} with less Dy addition. The magnetic properties, thermal stability, and the mechanism of H_{cj} enhancement have been studied.

2 Experimental

Commercial MQU-M magnetic powder with the nominal composition of $Nd_{22.3}Pr_{7.5}Fe_{bal}Co_{3.5}Ga_{0.46}B_{0.92}$ (wt%) was used as the starting materials. $Dy_{80}Fe_{20}$ (wt%) powder (particle size of approximately 200 μm) was prepared by induction melting, melt spinning, and grinding. $Dy_{80}Fe_{20}$ powder was mixed evenly with MQU-M powder with varying amounts (0, 0.5, 1.0, 1.5, and 2.0 wt%) and marked as DyFe-0.5, DyFe-1, DyFe-1.5, and DyFe-2, respectively. The mixed magnetic powder was hot-pressed at 650 °C under 250 MPa to prepare a fully dense isotropic magnet. Then the precursor was hot-deformed at 820 °C to obtain an anisotropic magnet with the dimension of Φ 24 × 3 mm. The degree of deformation $\varphi = (h_{begin} - h_{end}) / h_{begin}$ is approximately 73% (h_{begin} and h_{end} refer to the height of the sample before and after HD, respectively). The magnetic properties and recoil loops of HD magnets were measured by Physical Property Measurement System (PPMS, DynaCool, Quantum Design). The orientation degree of the HD magnets was studied by X-ray diffraction (XRD-Panalytical Empyrean). The microstructure and element distribution of the HD magnets were analyzed by scanning electron microscope (SEM-MIRA3 LMH) with an energy dispersive X-ray spectrometer (EDS).

3 Results and Discussion

Figure 1(a) shows the demagnetization curves of the original and DyFe doped magnets. The magnet prepared with pure MQU-M powder shows good magnetic properties of $H_{cj} = 12.55$ kOe, $J_r = 14.0$ kG, and $(BH)_{max} = 46.5$ MGOe. The H_{cj} of the DyFe doped magnets significantly improved to 14.25–18.23 kOe by doping 0.5 to 2.0 wt% DyFe. The increment of H_{cj} in the DyFe-2 doped magnet is 5.68 kOe, which shows an increase of 45.3%.

Figure 1(b) shows the initial magnetization curves and corresponding first derivative curves of HD magnets. In the initial stage of magnetization, the magnetization rises sharply because of the movement of magnetic domain walls within the plate-like grains. Then, the magnetic domain walls are pinned by the intergranular RE-rich phase with the increase of the magnetic field, resulting in a slow increase in magnetization [19]. When the force exerted by the magnetic field on the magnetic domain wall is greater than the pinning force, the magnetic domain wall escapes from the intergranular RE-rich phase, which leads to a sharp increase in magnetization [19, 20]. Subsequently, the magnetization gradually increases to saturation. The corresponding first derivative curves of all HD magnets show high initial susceptibility at low magnetic field, and the pinning field is very close to the H_{cj}, which indicates that the magnetic

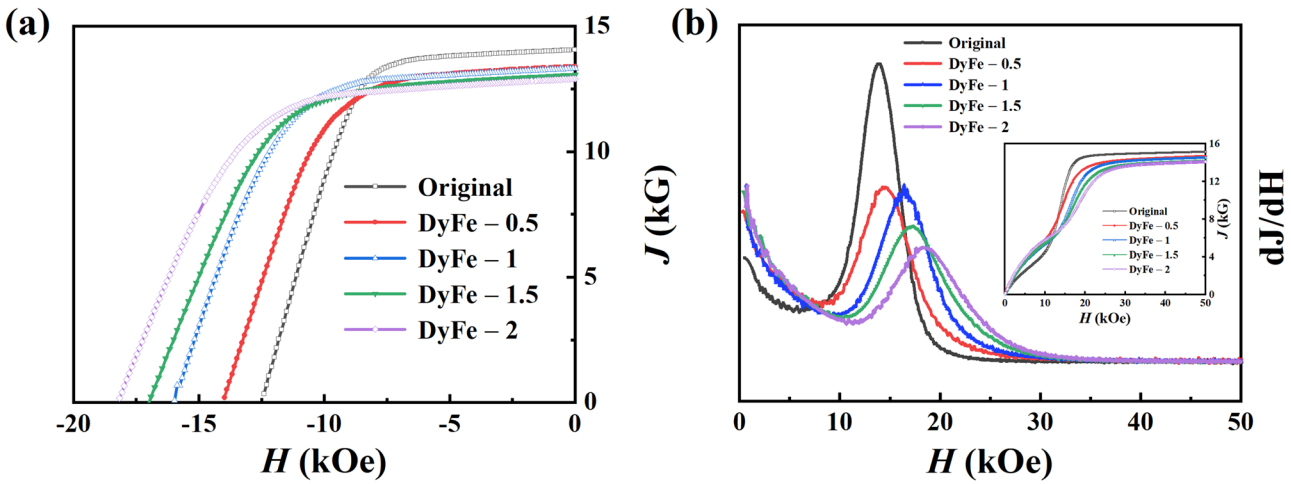

Fig. 1 (**a**) Demagnetization curves of the original and DyFe doped magnets. (**b**) Initial magnetization curves and the corresponding first derivative curves of the original and DyFe doped magnets

hardening mechanism of HD magnets is dominated by the domain wall pinning [21].

In order to study the thermal stability of the HD magnets doped with and without $Dy_{80}Fe_{20}$, we calculated the temperature coefficients of J_r (α) and H_{cj} (β) between 300 and 398 K according to the following equations [22]:

$$\alpha = \frac{J_r(T_1) - J_r(T_0)}{J_r(T_0)(T_1 - T_0)} \times 100\% \quad (1)$$

$$\beta = \frac{H_{cj}(T_1) - H_{cj}(T_0)}{H_{cj}(T_0)(T_1 - T_0)} \times 100\% \quad (2)$$

where T_1 and T_0 refer to high temperature and room temperature, respectively. Figure 2(a) and (b) show the temperature dependence of J_r and H_{cj} of the original and DyFe-2 doped magnets. The H_{cj} and J_r of DyFe-2 doped magnet are higher than those of the original magnet at different temperatures. The results show that the value of β increases from the original − 0.6319 to − 0.5290%/K, and the value of α also improves from − 0.1268 to − 0.1063%/K. The above results show that the DyFe addition has a positive effect on the thermal stability. The exchange coupling between grains, grain size, and the H_A of $Nd_2Fe_{14}B$ main phase play an important role for the improvement of the temperature coefficient of H_{cj}. In this work, the improvement of the temperature coefficient of H_{cj} is owing to the formation of (Nd, $Dy)_2Fe_{14}B$ around the main phase grains.

Figure 3 shows the M-T and corresponding first derivative curves of the original and DyFe-2 doped magnets. The T_C of the original and the DyFe-2 doped magnet is 621 K and 633 K, respectively. The thermal stability is improved due to the higher T_C of the DyFe-2 doped magnet. Dy diffuses into $Nd_2Fe_{14}B$ main phases and partially substitutes Nd sites to form (Nd, $Dy)_2Fe_{14}B$, increasing the T_C [23]. The T_C of $Nd_2Fe_{14}B$ is mainly determined by the exchange interaction between Fe–Fe. Yang et al. indicated that the exchange interaction between Fe–Fe atoms is improved by doping Dy, increasing the T_C of Nd-Fe-B magnets [24].

Figure 4 shows the XRD patterns on the surface perpendicular to the pressure direction of original and DyFe doped magnets. The texture of HD magnets is characterized by the value of $I_{(006)}/I_{(105)}$. A higher value of $I_{(006)}/I_{(105)}$ represents stronger texture [20, 25]. The orientation of texture is closely related to the J_r and $(BH)_{max}$. Note that the intensity of peak (006) is stronger than that of (105) in all HD magnets, indicating that all HD magnets have a good orientation degree. But, the orientation degree of the $Dy_{80}Fe_{20}$ doped magnets deteriorates gradually with the increasing content of $Dy_{80}Fe_{20}$, and the J_r and $(BH)_{max}$ decrease accordingly. The increase of liquid phase in the DyFe doped magnets leads to smaller deformation stresses, which causes the reduction of energy available during the solution-precipitation process [26]. As a result, there is no enough compressive stress to form the platelet-shaped $Nd_2Fe_{14}B$ grains. Furthermore, the reduction of viscosity of the GB phases deteriorates the texture due to the increasing liquid phase [27]. Therefore, the orientation degree of DyFe doped magnets become weak compared with the original magnet.

Figure 5(a1) and (b1) show the SEM micrographs of the original and DyFe-2 doped magnets. The microstructure of the HD magnets is composed of two regions: large grain layers with no orientation and fine grain layers with orientation. The distribution of large grain layers is periodic, and the total period of these layers is about 10–30 μm in the

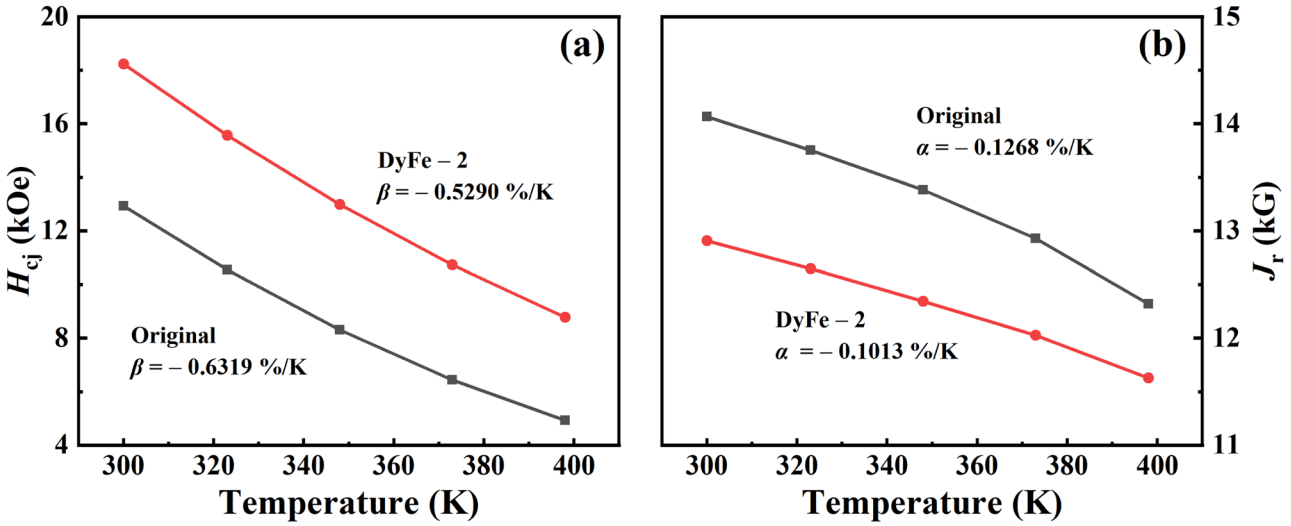

Fig. 2 Temperature dependence of H_{cj} (**a**) and J_r (**b**) of the original and DyFe-2 doped magnets at different temperature

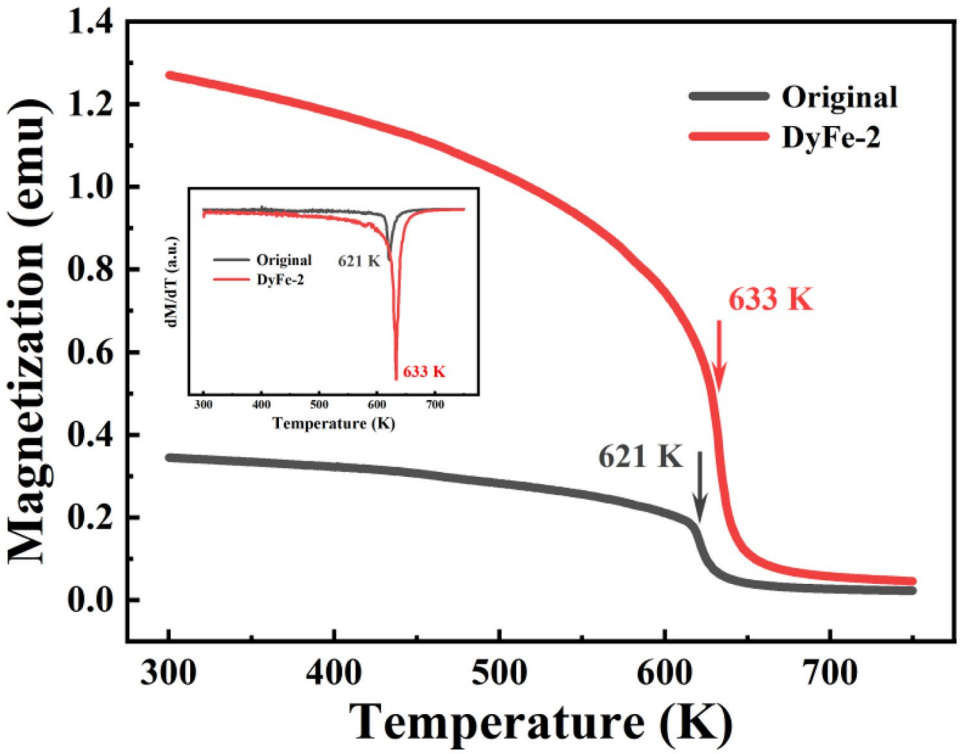

Fig. 3 The M-T and corresponding first derivative curves of the original and DyFe-2 doped magnets

original magnet. In contrary, there are no obvious periodic large grain layers in the DyFe-2 doped magnet, as shown in Fig. 5(b1) and (b2). The DyFe-2 doped magnet has an ultra-large grain layer with a thickness about 10–20 μm and a large grain layer with a thickness of 0.84 μm. During the heat treatment process, the increased RE-rich liquid phases in the DyFe-2 doped magnet accelerate the dissolution and migration of atoms. The non-oriented grains wrapped by the

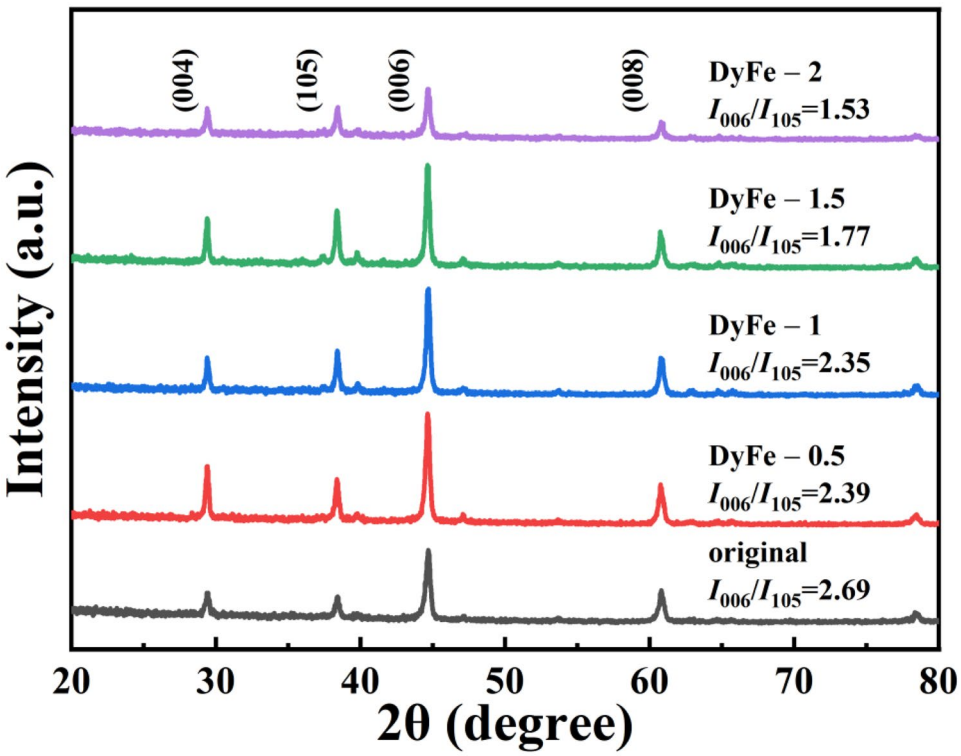

Fig. 4 XRD patterns of the original and DyFe doped magnets

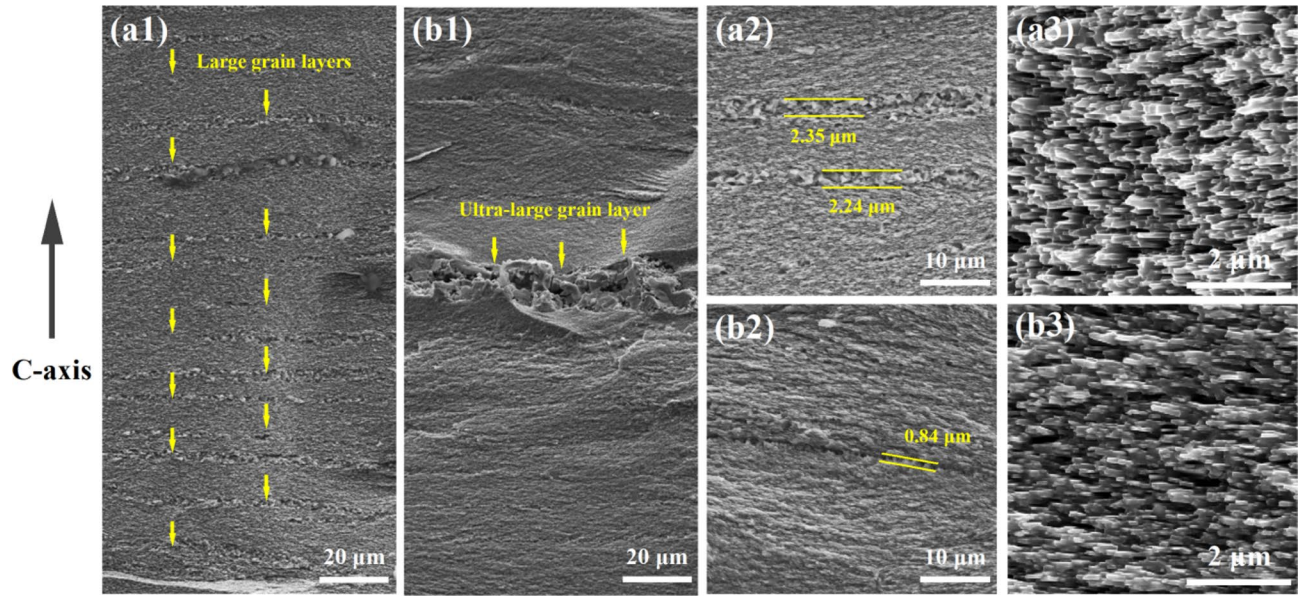

Fig. 5 The fracture SEM images of original (**a1**–**a3**) and DyFe-2 doped (**b1**–**b3**) magnets

liquid phase grow freely during precipitation, which forms the ultra-large grain layer at the ribbon interfaces of DyFe-2 doped magnet [28]. The fine grain layers consist of platelet-shaped $Nd_2Fe_{14}B$ grains with good orientation, as shown in Fig. 5(a3) and (b3). The unoriented $Nd_2Fe_{14}B$ grains in ultra-large grains layers affect the degree of texture of the DyFe-2 doped magnet, which is consistent with the decrease of J_r and $(BH)_{max}$.

Figure 6(a) and (b) show the cross-sectional SEM images of original and DyFe-2 doped magnets. The bright and black contrasts refer to the RE-rich phases and powder flakes, respectively. The fraction of periodic RE-rich phases

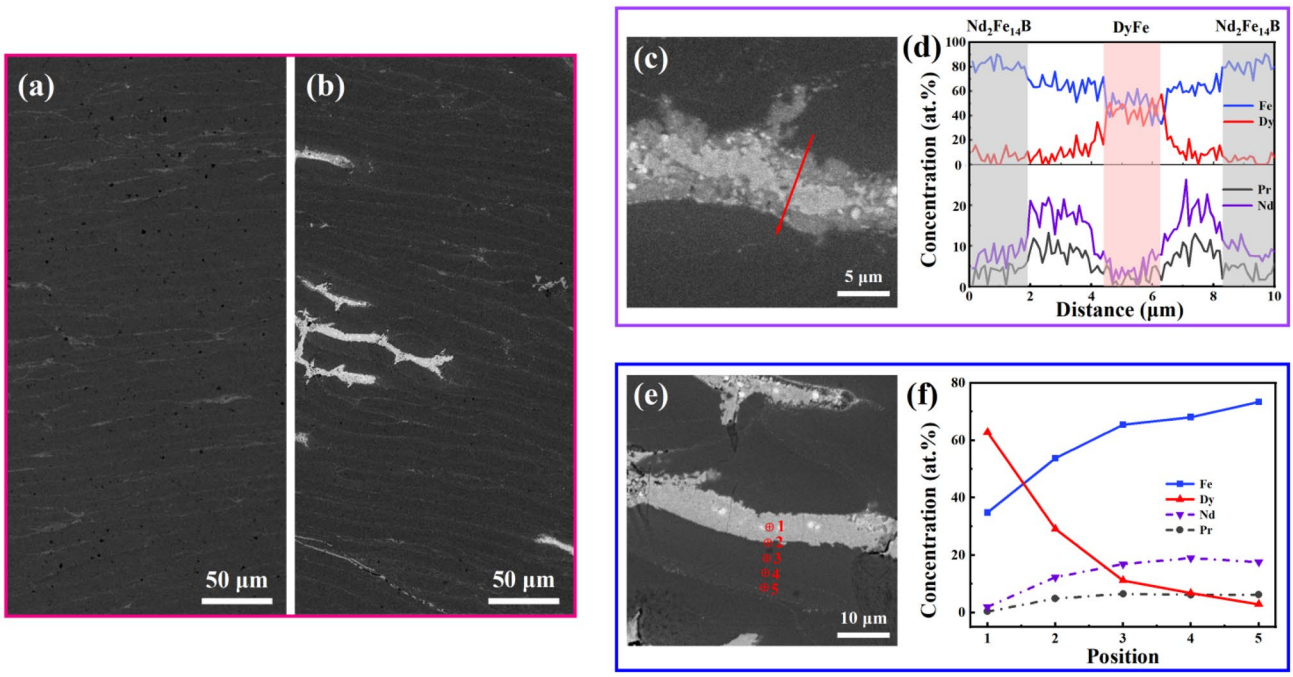

Fig. 6 (**a**) The cross-sectional SEM images of original magnet. (**b**–**f**) The cross-sectional SEM images and corresponding EDS analysis of DyFe-2 doped magnet

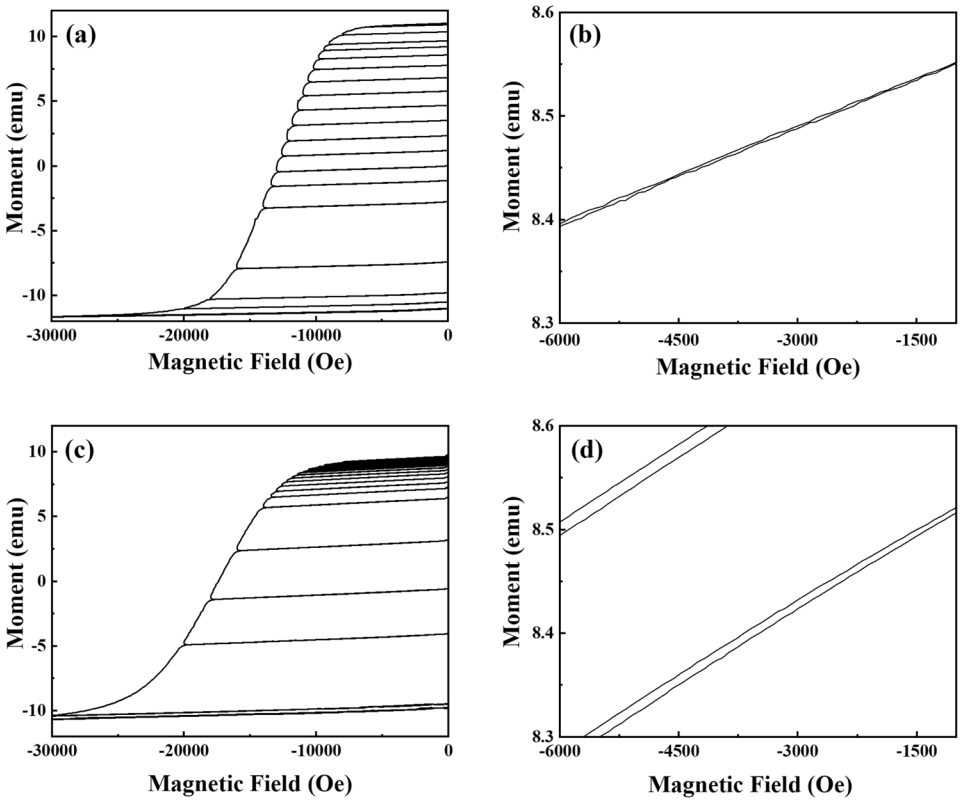

Fig. 7 The recoil loops of original (**a** and **b**) and DyFe-2 (**c** and **d**) doped magnets

increases obviously and surrounds the powder flakes after doping 2% $Dy_{80}Fe_{20}$. As shown in Fig. 6(c), the $Dy_{80}Fe_{20}$ additive easily squeezes into the gaps between powder flakes to form a diffusion layer. The corresponding EDS line scan in Fig. 6(d) shows that the $Dy_{80}Fe_{20}$ additive is surrounded by Nd-rich phase in the diffusion layer. During the thermal diffusion process, interdiffusion occurs between the $Dy_{80}Fe_{20}$ additive and matrix phase. The Dy diffuses from the $Dy_{80}Fe_{20}$ additive to the matrix phase and replaces Nd to form $(Nd, Dy)_2Fe_{14}B$ around the $Nd_2Fe_{14}B$ grains. Part of Nd atoms diffuses into the GB to form the RE-rich phase. The magnetic hardening is strengthened by the substitution of Dy for Nd, which greatly improves the H_{cj} of the DyFe-2 doped magnet. EDS point scans were performed to analyze the distribution of Dy, Pr, Nd, and Fe elements, as shown in Fig. 6(e) and (f). From points 1 to 5, the concentration of Dy decreases gradually, while the concentrations of Fe, Nd, and Pr increase gradually. The concentration gradients of Dy, Pr, Nd, and Fe indicate that the Dy continuously diffuses from the $Dy_{80}Fe_{20}$ additive to the matrix phase.

The recoil loops are used to simulate the change of magnetic properties in practical application [15]. The magnetizing and demagnetizing parts do not overlap in open recoil loops indicating energy loss of the magnet [29]. Figure 7(a, b) and (c, d) show the recoil loops and the local amplified regions of original and DyFe-2 doped magnets. The recoil loops are slightly open in the original magnet. While, the recoil loops of the DyFe-2 doped magnet are largely open, indicating an energy loss in the reverse magnetic field [29]. As shown in Fig. 6(a) and (b), there is almost no aggregation of RE-rich phases in the original magnet. While, the uneven RE-rich phases are aggregated between the powder flakes, causing uneven magnetic anisotropy and affecting the magnetic reversal mechanism of the DyFe-2 doped magnet. Therefore, the openness of the recoil loops is affected by the non-uniformly distributed RE-rich phases.

4 Conclusions

The magnetic properties, thermal stability, and microstructural features of the original and DyFe-2 doped magnet are studied. The conclusions are as follows:

(1) The Hcj of the DyFe-2 doped magnets greatly increased from the original 12.55 to 18.23 kOe, which shows an improvement of 5.68 kOe.
(2) The thermal stability of DyFe-2 doped magnet is improved. The temperature coefficient of Jr increases from − 0.1268 to − 0.1063%/K and that of Hcj increases from − 0.6319 to − 0.5290%/K. The T_C of DyFe-2 doped magnet increases from the original 621 to 633 K.
(3) Microstructural features showed that the better magnetic isolation by the RE-rich phase and the magnetic

hardening by (Nd, Dy)$_2$Fe$_{14}$B around the main grains are the main reasons for the enhancement of Hcj of the DyFe-2 doped magnet. The magnetic reversal mechanism is affected by the uneven aggregation of RE-rich phases, which causes the large openness of the recoil loops.

Funding This work was supported by the National Natural Science Foundation of China (51561009), the Natural Science Foundation of Jiangxi Province (20192BAB206004), the Key Research and Development Program of Jiangxi Province (20202BBE53014), the Foundation of Jiangxi Education Department (GJJ200832), and the Open Foundation of Guo Rui Scientific Innovation Rare Earth Functional Materials Co, Ltd. (KFJJ-2019–0004).

References

1. Matsuura, Y.: Recent development of Nd-Fe-B sintered magnets and their applications. J. Magn. Magn. Mater. **303**, 344–347 (2006). https://doi.org/10.1016/j.jmmm.2006.01.171
2. Satoh, H., Akutsu, A., Miyamura, T., Shinoki, H.: Development of traction motor for fuel cell vehicle, SAE Technical Paper Series 2004–01–0567, SAE Int. Warrendale, PA, (2004). https://doi.org/10.4271/2004-01-0567
3. Honjo, S., Iwai, A., Suzumori, H., Okamura, M.: Development of traction motor for new fuel cell vehicle and new electric vehicle, SAE Technical Paper Series 2018–01–0450, SAE Int. Warrendale, PA, (2018). https://doi.org/10.4271/2018-01-0450
4. Oono, N., Sagawa, M., Kasada, R., Matsui, H., Kimura, A.: Production of thick high-performance sintered neodymium magnets by grain boundary diffusion treatment with dysprosium–nickel–aluminum alloy. J. Magn. Magn. Mater. **323**, 297–230 (2011). https://doi.org/10.1016/j.jmmm.2010.09.021
5. Hirosawa, S., Matsuura, Y., Yamamoto, H., Fujimura, S., Sagawa, M.: Magnetization and magnetic anisotropy of $R_2Fe_{14}B$ measured on single crystals. J. Appl. Phys. **59**, 873 (1986). https://doi.org/10.1063/1.336611
6. Li, J.J., Huang, X.Y., Zeng, L.L., Ouyang, B., Yu, X.Q., Yang, M.N., Yang, B., Rawat, R.S., Zhong, Z.C.: Tuning magnetic properties, thermal stability and microstructure of NdFeB magnets with diffusing Pr-Zn films. J. Mater. Sci. Technol. **41**, 81–87 (2020). https://doi.org/10.1016/j.jmst.2019.09.024
7. Li, J.J., Guo, C.J., Zhou, T.J., Qi, Q.Z., Yu, X., Yang, B., Zhu, M.G.: Effects of diffusing DyZn film on magnetic properties and thermal stability of sintered NdFeB magnets. J. Magn. Magn. Mater. **454**, 215–220 (2018). https://doi.org/10.1016/j.jmmm.2018.01.070
8. Zhong, S.W., Yang, M.N., Rehman, S.U., Lu, Y.J., Li, J.J., Yang, B.: Microstructure, magnetic properties and diffusion mechanism of DyMg co-deposited sintered Nd-Fe-B magnets. J. Alloys Compd. **819**, 153002 (2020). https://doi.org/10.1016/j.jallcom.2019.153002
9. Lee, W.R.: Hot-pressed neodymium-iron-boron magnets. Appl. Phys. Lett. **46**, 790–791 (1985). https://doi.org/10.1063/1.95884
10. Zhang, T.Q., Xing, W.D., Chen, F.G., Zhang, L.T., Yu, R.: Improvement of coercivity and its thermal stability of hot-deformed Nd-Fe-B magnets processed by $Tb_{70}Cu_{30}$ doping and subsequent $Nd_{85}Cu_{15}$ diffusion. Acta. Mater. **220**, 117296 (2021). https://doi.org/10.1016/j.actamat.2021.117296
11. Zhang, T.Q., Chen, F.G., Zheng, Y., Wen, H.Y., Zhang, L.T., Zhou, L.G.: Anisotropic behavior of grain boundary diffusion in hot-deformed Nd-Fe-B magnet. Scr. Mater. **129**, 1–5 (2017). https://doi.org/10.1016/j.scriptamat.2016.10.017
12. Zeng, H.X., Liu, Z.W., Li, W., Zhang, J.S., Zhao, L.Z., Zhong, X.C., Yu, H.Y., Guo, B.C.: Significantly enhancing the coercivity of NdFeB magnets by ternary Pr-Al-Cu alloys diffusion and understanding the elements diffusion behavior. J. Magn. Magn. Mater. **471**, 97–104 (2019). https://doi.org/10.1016/j.jmmm.2018.09.080
13. Liu, Q.B., Tang, X., Chen, R.J., Wang, Z.X., Ju, J.Y., Yin, Z.W., Yan, A.R., Xu, H.: Effect of Tb-Fe diffusion on magnetic properties and thermal stability of hot-deformed magnets. J. Alloys Compd. **773**, 1108–1113 (2019). https://doi.org/10.1016/j.jallcom.2018.09.205
14. Jing, Z., Guo, Z.H., He, Y.N., Zhang, M.L., Wang, X., Zhu, M.G., Li, W.: Coercivity enhancement of nanocrystalline hot-deformed Nd-Fe-B magnets by low melting eutectic MM-Cu (MM = La, Ce, Pr, Nd) alloys addition. J. Rare Earths. **38**, 594–599 (2020). https://doi.org/10.1016/j.jre.2019.04.024
15. Huang, X.Y., Li, J.J., Rehman, S.U., Qu, P.P., He, L., Zeng, L.L., Yu, X.Q., Yang, M.N., Zhong, Z.C.: Microstructure evolution and coercivity enhancement in $Pr_{50}Dy_{20}Cu_{15}Ga_{15}$-doped hot-deformed Nd-Fe-B magnets. J. Magn. Magn. Mater. **503**, 166637 (2020). https://doi.org/10.1016/j.jmmm.2020.166637
16. Tang, X., Chen, R.J., Yin, W.Z., Wang, J.Z., Tang, Xu., Lee, D., Yan, A.R.: Enhanced texture in die-upset nanocomposite magnets by Nd-Cu grain boundary diffusion. Appl. Phys. Lett. **102**, 072409 (2013). https://doi.org/10.1063/1.4793429
17. Sawatzki, S., Dirba, I., Schultz, L., Gutfleisch, O.: Electrical and magnetic properties of hot-deformed Nd-Fe-B magnets with different DyF_3 additions. J. Appl. Phys. **114**, 133902 (2013). https://doi.org/10.1063/1.4822026
18. Liu, L.H., Sepehri-Amin, H., Sasaki, T.T., Ohkubo, T., Yano, M., Sakuma, N., Kato, A., Shoji, T., Hono, K.: Coercivity enhancement of Nd-Fe-B hot-deformed magnets by the eutectic grain boundary diffusion process using Nd-Ga-Cu and Nd-Fe-Ga-Cu alloys. AIP Adv. **8**, 056205 (2018). https://doi.org/10.1063/1.5006575
19. Sepehri-Amin, H., Ohkubo, T., Gruber, M., Schrefl, T., Hono, K.: Micromagnetic simulations on the grain size dependence of coercivity in anisotropic Nd–Fe–B sintered magnets. Scr. Mater. **89**, 29–32 (2014). https://doi.org/10.1016/j.scriptamat.2014.06.020
20. Tang, X., Chen, R.J., Yin, W.Z., Jin, C.X., Lee, D., Yan, A.R.: The magnetization behavior and open recoil loops of hot-deformed Nd-Fe-B magnets infiltrated by low melting point PrNd-Cu alloys. Appl. Phys. Lett. **107**, 202403 (2015). https://doi.org/10.1063/1.4936154
21. Li, Y.Q., Xu, X.C., Yue, M., Wu, D., Liu, W.Q., Zhang, D.T.: Effect of heterogeneous microstructure on magnetization reversal mechanism of hot-deformed Nd-Fe-B magnets. J. Rare Earths. **37**, 1088–1095 (2019). https://doi.org/10.1016/j.jre.2019.03.009
22. Rehman, S.U., Song, J., Jiang, Q.Z., He, L.K., Xie, W.C., Zhong, Z.C.: Magnetic properties, phase transition temperatures, intergranular exchange interactions and microstructure of Ta-doped Nd-Ce-Fe-B nano ribbons. J. Supercond. Novel Magn. **33**, 877–882 (2020). https://doi.org/10.1007/s10948-019-05259-6
23. Yan, G.H., Chen, R.J., Ding, Y., Guo, S., Lee, D., Yan, A.R.: The preparation of sintered NdFeB magnet with high-coercivity and high temperature-stability, J. Phys.: Conf. Ser. **266**, 012052 (2011). https://doi.org/10.1088/1742-6596/266/1/012052

24. Yang, M.N., Wang, H., Hu, Y.F., Yang, L.Y., Maclennan, A.: Relating atomic local structures and Curie temperature of NdFeB permanent magnets: an X-ray absorption spectroscopic study, Rare Met. (Beijing, China). **37**, 983–988 (2018). https://doi.org/10.1007/s12598-017-0918-5
25. Wang, Z.X., Pei, K., Zhang, J.J., Chen, R.J., Xia, W.X., Wang, J.Z., Li, M., Yan, A.R.: Correlation between the microstructure and magnetic configuration in coarse-grain inhibited hot-deformed Nd-Fe-B magnets. Acta Mater. **167**, 103 (2019). https://doi.org/10.1016/j.actamat.2019.01.025
26. Liesert, S., Kirchner, A., Grunberger, W., Handstein, A., Rango, P.D., Fruchart, D., Schultz, L., Muller, K.H.: Preparation of anisotropic NdFeB magnets with different Nd contents by hot deformation (die-upsetting) using hot-pressed HDDR powders, J. Alloys Compd. **266**, 260–265 (1998). https://doi.org/10.1016/S0925-8388(97)00439-8
27. Lee, Y.I., Huang, G.Y., Shih, C.W., Chang, W.C., Chang, H.W., You, J.S.: Coercivity enhancement in hot deformed $Nd_2Fe_{14}B$-type magnets by doping low-melting RCu alloys (R = Nd, Dy, Nd + Dy). J. Magn. Magn. Mater. **439**, 1–5 (2017). https://doi.org/10.1016/j.jmmm.2017.05.009
28. Lai, B., Li, Y.F., Wang, H.J., Li, A.H., Zhu, M.G., Li, W.: Quasi-periodic layer structure of die-upset NdFeB magnets. J. Rare Earths. **31**, 679–684 (2013). https://doi.org/10.1016/S1002-0721(12)60342-1
29. Hou, Y.H., Wang, Y.L., Huang, Y.L., Wang, Y., Li, S., Ma, S.C., Liu, Z.W., Zeng, D.C., Zhao, L.Z., Zhong, Z.C.: Effects of Nd-rich phase on the improved properties and recoil loops for hot deformed Nd-Fe-B magnets, Acta Mater. **115**, 385e391 (2016). https://doi.org/10.1016/j.actamat.2016.06.015